Assessing diabetic foot ulcer development risk with hyperspectral tissue oximetry

Dmitry Yudovsky,[a] Aksone Nouvong,[b] Kevin Schomacker,[c] and Laurent Pilon[a]
[a]University of California, Los Angeles, Henry Samueli School of Engineering and Applied Science Biomedical Inter-Department Program, Los Angeles, California 90095-1597
[b]UCLA/Olive View Medical Center and Western University Healthcare Center, Department of Surgery, Sylmar, California 91342-1495
[c]HyperMed Inc., Burlington, Massachusetts 01803

Abstract. Foot ulceration remains a serious health concern for diabetic patients and has a major impact on the cost of diabetes treatment. Early detection and preventive care, such as offloading or improved hygiene, can greatly reduce the risk of further complications. We aim to assess the use of hyperspectral tissue oximetry in predicting the risk of diabetic foot ulcer formation. Tissue oximetry measurements are performed during several visits with hyperspectral imaging of the feet in type 1 and 2 diabetes mellitus subjects that are at risk for foot ulceration. The data are retrospectively analyzed at 21 sites that ulcerated during the course of our study and an ulceration prediction index is developed. Then, an image processing algorithm based on this index is implemented. This algorithm is able to predict tissue at risk of ulceration with a sensitivity and specificity of 95 and 80%, respectively, for images taken, on average, 58 days before tissue damage is apparent to the naked eye. Receiver operating characteristic analysis is also performed to give a range of sensitivity/specificity values resulting in a Q-value of 89%. [DOI: 10.1117/1.3535592]

Keywords: hyperspectral imaging; diabetic foot ulcers; tissue oximetry; medical screening technology; wound diagnostics; wound care.

Paper 10086RR received Feb. 19, 2010; revised manuscript received Dec. 14, 2010; accepted for publication Dec. 17, 2010; published online Feb. 11, 2011.

1 Introduction

Diabetes mellitus affects 194 million people worldwide[1] and is expected to increase in prevalence to 439 million by the year 2030.[2] Foot ulceration is a major complication that occurs in as many as 15–25% of type 1 and 2 patients with diabetes mellitus over their lifetime.[3,4] If left untreated, foot ulcers may become infected and develop deep tissue necrosis, which may require amputation.[5] In fact, foot ulcers precede roughly 85% of all lower extremity amputations in patients with diabetes mellitus[5] and more than 88×10^3 lower limb amputations are performed annually on diabetic patients in the United States.[6] The cost of foot disorder diagnosis and management is estimated to be >\$6 billion annually in the United States.[7,8] Furthermore, it has been suggested that 40%–85% of diabetic foot amputations can be avoided with early detection and preventive techniques such as offloading and improved hygiene.[9] Automated early identification of tissue at risk of ulcerating may enable directed care, thereby reducing the incidence of foot ulceration and amputation. This study proposes to use hyperspectral imaging as a screening tool for detecting tissue at risk of diabetic foot ulcers before tissue damages become apparent to a care giver in a clinical setting.

2 Background

2.1 *Diabetic Foot Ulcers*

Prolonged and poorly controlled diabetes irreparably damages bodily tissues. Nerve damage in the lower limbs results in diabetic neuropathy, whereby the patient's somatosensory and autonomic function are diminished or completely lost.[10] The subsequent loss of protective sensation, impaired gait control, bone deformities (e.g., Charcot foot), callus formation, and/or inhibited sweat response result in excessive shear and pressure that damages the diabetic foot.[10,11] Furthermore, 10–40% of diabetic patients are afflicted with peripheral vascular disease.[12] Typically, the vessels that carry blood to the legs, arms, stomach, or kidneys narrow due to inflammation or tissue damage, resulting in impaired blood flow.[12] Thus, repeated trauma to the foot in conjunction with inhibited protective or healing response due to denervation and/or poor vascularization increases the risk of foot ulceration in diabetic patients.[10]

2.2 *Medical Hyperspectral Imaging*

Hyperspectral imaging consists of recording a series of images representing the intensity of diffusely reflected light from biological tissue at discrete wavelengths λ_j.[13] The resulting set of images is called a hypercube, denoted by $H(x, y, \lambda_j)$, where x and y are the two spatial coordinates and λ_j is the spectral coordinate. Each pixel in a hypercube corresponds to the diffuse reflectance spectrum of the tissue at a location (x, y). Analysis of the hypercube can reveal the local concentration of tissue chromophores, such as melanin or hemoglobin.[13,14]

Hemoglobin is the molecule in blood responsible for oxygen transport from the lungs to the rest of the body. In its oxygen-bounded and unbounded forms, hemoglobin is called oxyhemoglobin and deoxyhemoglobin, respectively. The ratio of oxyhemoglobin concentration to the total hemoglobin

Address all correspondence to Laurent Pilon, Mechanical and Gerospace Engineering, University of California, Los Angeles, 37-132, Engineering IV, 420 Westwood Plaza, Los Angeles, California 90095. Tel: 310-206-5598; Fax: 310-206-4830; E-mail: pilon@seas.ucla.edu

1083-3668/2011/16(2)/026009/8/\$25.00 © 2011 SPIE

concentration in the blood is the so-called oxygen saturation denoted by SO_2. It indicates the rate of oxygen delivery to and consumption by the tissues. The optical extinction coefficient of oxyhemoglobin differs significantly from that of deoxyhemoglobin.[15] Thus, the spectral absorption coefficient of tissue depends on the concentration and oxygen saturation of hemoglobin within the tissue. Furthermore, changes in the tissue's spectral absorption coefficient change its diffuse reflectance spectrum. Thus, using the hyperspectral imaging technique, known as transcutaneous tissue oximetry, it is possible to estimate the hemoglobin concentration and oxygen saturation from the tissue's diffuse reflectance.[13]

Recently, hyperspectral imaging in the visible and near-infrared parts of the spectrum has been used to determine the spatial distribution of oxygen saturation in human skin[13,16,17] and to detect the circulatory changes in the diabetic foot.[18–20] Nouvong et al.[18] enrolled 66 type 1 and type 2 diabetic subjects and followed them for up to 18 months. Nouvong et al.[18] evaluated hyperspectral imaging as a tool for predicting the healing potential of diabetic foot ulcers. In brief, 54 of the enrolled subjects completed the study. Each subject had one or more diabetic foot ulcer(s) at the beginning of the study. Hyperspectral tissue oximetry measurements of these subjects' feet were performed every two weeks for up to 18 months or until the ulcer healed. Then, ulcers were manually classified into one of two groups namely (*i*) ulcers that healed within 24 weeks and (*ii*) ulcers that did not heal within 24 weeks. Periwound-averaged oxyhemoglobin and deoxyhemoglobin concentrations as well as oxygen saturation were calculated around nonhealing ulcers and found, on average, to be respectively 25, 6.8, and 10% smaller than those estimated around healing ulcers. Based on oximetry data gathered from all 54 subjects and averaged over the periwound areas, Nouvong et al.[18] developed a statistical algorithm that automatically classified ulcers as healing or non-healing. The algorithm exhibited a sensitivity and specificity of 80 and 74%, respectively.[18]

The set of hyperspectral data analyzed in this study was selected from that data gathered by Nouvong et al.[18] By contrast, the present study retrospectively analyzes hyperspectral images of diabetic feet collected prior to ulceration. In other words, although the results of both studies stem from the same data set, the subsets of data used by Nouvong et al.[18] differ from that used in the present study in that the hyperspectral images were taken at different times.

3 Materials and Methods

3.1 *Experimental Apparatus*

The hyperspectral imager used in this study is schematically depicted in Fig. 1. The illumination optics consisted of seven broadband visible light-emitting diodes [(LEDs), XRE WHT-L1 by CREE Incorporated, Durham, North Caroline] emitting primarily between 500 and 700 nm, and of collimating wide lenses (OP-025 by Dialight Corp., North Yorkshire, UK). The LEDs were arranged radially around the collection optics and cross-polarized relative to it to reduce specular reflections (glare) in the images. This was achieved by placing a linear polarizer film (XP38 by Optical Filters Limited, Meadville, Pennsylvania), set between two acrylic sheets, in front of the LEDs assembly. The collection optics were composed of (*i*) a

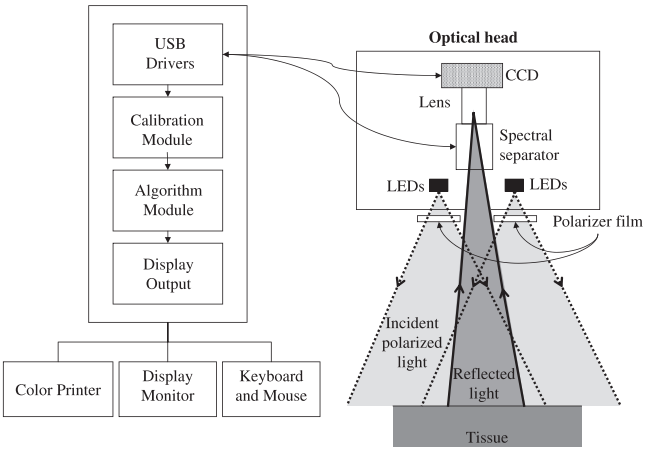

Fig. 1 Schematic of the different components of the hyperspectral imager (OxyVu™ by HyperMed Incorporated).

spectral separator (LCTF-10-20 by CRI Incorporated, Woburn, Massachusetts), (*ii*) a charged-coupled device [(CCD), Guppy F-1468 by Applied Vision Technology, Stadtroda, Germany], and (*iii*) a 25-mm focal-length imaging lens (MFA2514 by SenkoADL, Marlboro, Massachusetts). The spectral separator was tunable over the range of 400–720 nm with a full-width-at-half-maximum (FWHM) value of 10 nm. It also acted as a linear polarizer. The system was designed with an 18-in. focal length and had a spatial resolution of 100 μm. Figure 2 shows a photograph of the actual experimental apparatus OxyVu™ device.

For each measurement site, the hyperspectral imager collected two hypercubes corresponding to either background or LED illuminated conditions denoted by $B_{\text{tissue}}(x, y, \lambda_j)$ and $I_{\text{tissue}}(x, y, \lambda_j)$, respectively. The spectral separator was tuned to 15 equally spaced wavelengths between 500 and 660 nm while the CCD measured the tissue reflectance. The LEDs were switched off and on to produce both illumination conditions, respectively. Acquisition at each wavelength lasted for $\sim$1 s.

To normalize and correct for spectral variation in illumination intensity and collector sensitivity, the hyperspectral imager was calibrated to a well-characterized highly reflective diffuse reflectance standard (Check Pad, HyperMed, Incorporated) prior to imaging every subject. The same procedure as above was used to acquire background and illuminated calibration hypercubes denoted by $B_{\text{calib}}(x, y, \lambda_j)$ and $I_{\text{calib}}(x, y, \lambda_j)$, respectively. Note that $I_{\text{calib}}(x, y, \lambda_j)$ was gathered under combined background and LED illuminations and was thus relatively much larger than $B_{\text{calib}}(x, y, \lambda_j)$, which was gathered under background illumination only. Therefore, the noise associated with background illumination was expected to be small. Then, the so-called apparent absorption of the tissue $A(x, y, \lambda_j)$ at the spatial coordinate (x, y) and wavelength λ_j was calculated using the modified Beer–Lambert's law as,[21]

$$A_{\text{obs}}(x, y, \lambda_j) = -\log_{10}\left[\frac{I_{\text{tissue}}(x, y, \lambda_j) - B_{\text{tissue}}(x, y, \lambda_j)}{I_{\text{calib}}(x, y, \lambda_j) - B_{\text{calib}}(x, y, \lambda_j)}\right]. \quad (1)$$

The primary chromophores in the human skin responsible for absorption of visible light are oxyhemoglobin, deoxyhemoglobin,

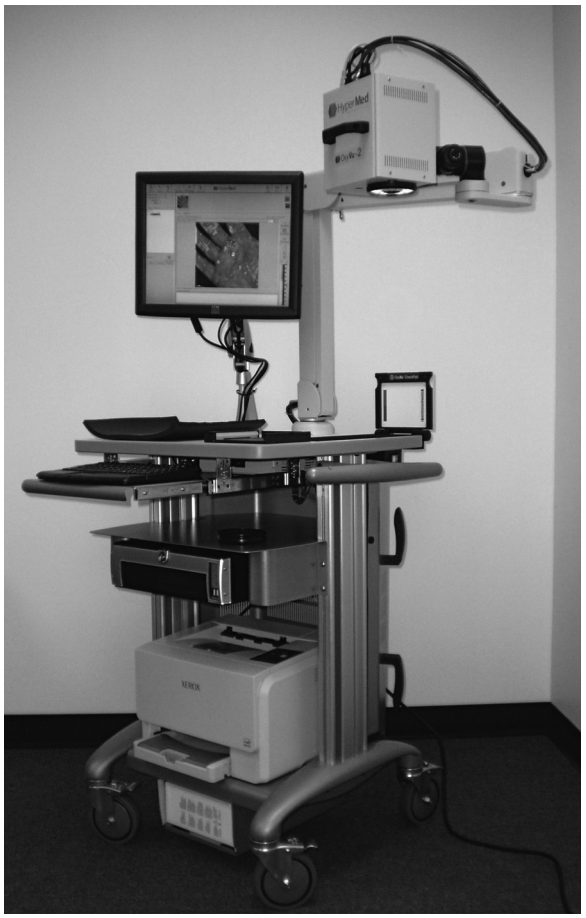

Fig. 2 Photograph of the hyperspectral imager OxyVu™ (by HyperMed Incorporated) used in this study.

and melanin.[22–24] Thus, the apparent absorption was approximated as the sum of absorption contributions from tissue chromophores as well as scattering by the tissue,[21]

$$A_{\mathrm{mod}}(x, y, \lambda_j) = M_{\mathrm{oxy}}(x, y) L \epsilon_{\mathrm{oxy}}(\lambda_j) + M_{\mathrm{deoxy}}(x, y) \times L \epsilon_{\mathrm{deoxy}}(\lambda_j) + M_{\mathrm{mel}}(x, y) L \epsilon_{\mathrm{mel}}(\lambda_j) + G, \quad (2)$$

where $M(x, y)$ is a molar concentration at coordinate (x, y) (or μmol/L) and $\epsilon(\lambda)$ is a spectral molar extinction coefficient [in $\mathrm{cm}^{-1}/(\mu\mathrm{mol/L})$] while the subscripts "oxy," "deoxy," and "mel" refer to oxyhemoglobin, deoxyhemoglobin, and melanin, respectively. The mean-free path L (in centimeters) is the average distance traveled by a photon within the tissue before it is diffusely reflected due to multiple scattering within the tissue.[21] The term G accounted for light scattering by the tissue outside of the acceptance angle of the collector optics. It depends on the geometry of the collector optics[25] and was assumed to be independent of wavelength.[22] The spectral molar extinction coefficients $\epsilon_{\mathrm{oxy}}(\lambda_j)$, $\epsilon_{\mathrm{deoxy}}(\lambda_j)$, and $\epsilon_{\mathrm{mel}}(\lambda_j)$ were taken from the literature.[26–29] The mean-free path L was unknown, and thus, the products $M_{\mathrm{oxy}}(x, y)L$, $M_{\mathrm{deoxy}}(x, y)L$, and $M_{\mathrm{mel}}(x, y)L$ were replaced by unitless effective concentrations $\mathrm{OXY}(x, y)$, $\mathrm{DEOXY}(x, y)$, and $\mathrm{MEL}(x, y)$, respectively. Then, the four unknown parameters OXY, DEOXY, MEL, and G were retrieved at each location (x, y) by minimizing the residual r defined as follows:

$$r = \sum_{j=1}^{15} \{A_{\mathrm{exp}}(\lambda_j) - s[\mathrm{OXY}\epsilon_{\mathrm{oxy}}(\lambda_j) + \mathrm{DEOXY}\epsilon_{\mathrm{deoxy}}(\lambda_j) + \mathrm{MEL}\epsilon_{\mathrm{mel}}(\lambda_j)] + G\}^2, \quad (3)$$

where the factor s (measured in $\mu\mathrm{mol/L/cm}^{-1}$) was introduced to scale the effective oxyhemoglobin concentration OXY to be 50, on average, for a population of healthy subjects. Minimization was performed numerically with the Levenberg–Marquardt algorithm.[30] The effective total hemoglobin concentration HEME and the oxygen saturation SO_2 at coordinate (x, y) were calculated as $\mathrm{HEME} = \mathrm{OXY} + \mathrm{DEOXY}$ and $\mathrm{SO}_2 = \mathrm{OXY/HEME}$, respectively. For the sake of clarity, the coordinates (x, y) have been omitted.

The OXY and DEOXY values reported by OxyVu were validated against those obtained from high-resolution spectrometric measurements and retrieving of M_{oxy} and M_{deoxy} in units of mmol/L in a manner similar to that described by Zonios et al.[31] Oximetry data were gathered simultaneously with both devices from eight anatomical sites pre- and postpressure cuff-induced ischemia on the dorsal feet of 19 healthy subjects. The values of OXY and DEOXY were found to be linearly proportional to M_{oxy} and M_{deoxy} with correlation coefficients of 0.86 and 0.88, respectively. This confirms that the OXY and DEOXY values reported by OxyVu are strong indicators of the actual molar concentrations of oxyhemoglobin and deoxyhemoglobin, albeit in arbitrary units. The experimental apparatus and the data analysis used in this study were developed and successfully validated by Zuzak et al.[13] for tissue oximetry under wide-field illumination. Additionally, other investigators have used similar devices to perform hyperspectral tissue oximetry with wide-field illumination.[17,32,33]

3.2 *Procedure and Data Selection*

Hyperspectral tissue oximetry data gathered from 66 subjects at the Olive View Medical Center (Olive View-UCLA IRB No. 05H-609300) and reported in detail in Ref. 18 was analyzed in this study. Subjects were imaged supine on a standard examination table or reclining chair. A fiducial target was placed near the center of the imager's field of view to correct for movement of the foot during the image acquisition.

Hyperspectral tissue oximetry data from diabetic subjects (*i*) who developed foot ulcers and (*ii*) who never exhibited ulceration during the study period were examined. The first set provided images of preulcer locations and could be used to test the sensitivity of the prediction algorithm. Visible images of newly formed ulcers were studied, and the approximate location and size of the ulcer was recorded. The second set provided images of locations that were at risk of developing ulcers but were known not to have developed ulcers during the entire period of the study. These images were used to test the specificity of the algorithm. However, data from patients who exhibited ulcers at the beginning of the study were not examined because no image of the affected sites prior to ulceration were available. Therefore, data from these patients could not be used to assess the algorithm's performance. Previous images of the same

anatomical location were examined to retrospectively analyze the tissue oximetry data from the site before the lesions formed.[18] Finally, prior to image analysis, regions known to cause unreliable OXY and DEOXY values were identified and omitted during analysis. They included fingernails, the fiducial target, open wounds, the image background, and areas where the tissue was oblique to the imaging plane. Matlab™ was used to facilitate image processing.

3.3 *Analysis of Tissue Oximetry Data*

Figures 3(a) and 3(b) show typical photographs of the left foot toes and plantar area of the foot after and before a diabetic foot ulcer formed on the plantar surface of the subject's foot, respectively. These two photographs were taken 116 days apart. Figure 3(b) shows the area around the undeveloped ulcer divided into (i) a target region denoted by T and (ii) an adjacent region divided into eight identical segments denoted by $(C_k)_{1\leq k\leq 8}$. The target area T was centered on the area where the ulcer eventually formed as determined from Fig. 3(a). The diameter of the target region T was chosen to be 1 cm, which was larger than most newly developed ulcers found in this study. The inner rim of the adjacent region [Fig. 3(b)] was 1 cm from the outer rim of the target region. The same target dimension was used for ulcers with diameters of >1 cm diam. These choices were based on clinical experience and previous studies predicting the healing potential of already formed diabetic foot ulcers.[18] However, the edge of the target was aligned with the edge of the site known to have ulcerated such that at least half of the adjacent segments were located outside the site. The radius of the outer rim of the adjacent region was chosen such that the surface area of each of the eight segments was the same as the of the target and equal to 0.79 cm^2.

The maximum differences (MD) in oxyhemoglobin and deoxyhemoglobin concentrations between the target T and the adjacent regions were defined as

$$\mathrm{MD(OXY)} = \mathrm{OXY}_T - \mathrm{OXY}_{k_{\mathrm{OXY}}} \tag{4}$$

$$\mathrm{MD(DEOXY)} = \mathrm{DEOXY}_T - \mathrm{DEOXY}_{k_{\mathrm{DEOXY}}} \tag{5}$$

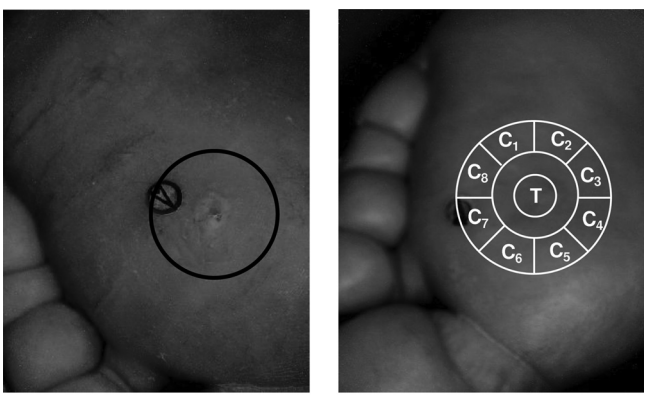

(a) (b)

Fig. 3 (a) Image of plantar ulcer (circled) developed on the foot of an affected diabetic subject. (b) Image of the same foot without ulceration 116 days earlier. Target and adjacent region centered on the location of the affected area are not drawn to scale.

where OXY_T or DEOXY_T and $\mathrm{OXY}_{k_{\mathrm{OXY}}}$ or $\mathrm{DEOXY}_{k_{\mathrm{DEOXY}}}$ were the average oxyhemoglobin or deoxyhemoglobin concentrations in the target and adjacent regions with indices k_{OXY} or k_{DEOXY}, respectively. The indices k_{OXY} and k_{DEOXY} in Eqs. (4) and (5) were chosen to maximize the absolute values of MD(OXY) and MD(DEOXY), respectively. Typically, k_{OXY} and k_{DEOXY} were the same (i.e., they corresponded to the same adjacent region). Note that the values of |MD(OXY)| and |MD(DEOXY)| between the target and any of the adjacent regions were systematically larger at affected sites than elsewhere on the foot. Sensitivity was calculated by dividing the area of skin accurately classified as affected by the total surface area of the affected foot. Specificity was calculated by dividing the total area of skin that was accurately classified as unaffected for comparative subjects by the total area of skin for both feet of affected and comparative subjects.

The physiological premise of calculating MD values relied on detecting hyperperfusion or hypovascularization associated with inflammation and ischemia in the target region, respectively. It was hypothesized that ulceration due to ischemia may result in hypovascular tissue and, thus, diminished oxyhemoglobin and deoxyhemoglobin concentrations in the affected site when compared to nearby unaffected tissue. Therefore, ischemic areas would exhibit negative values of MD(OXY) and MD(DEOXY) with large absolute values. On the other hand, ulceration accompanied by inflammation may result in hyperperfusion and, thus, larger oxyhemoglobin and deoxyhemoglobin concentrations in the affected site when compared to nearby unaffected tissue. Therefore, inflamed areas would exhibit positive values of MD(OXY) and MD(DEOXY) with large absolute values. Thus, we hypothesized that the absolute values |MD(OXY)| and |MD(DEOXY)| calculated at an ischemic or inflamed site should be larger than values calculated elsewhere on the foot or at locations on feet that did not form ulcers.

4 Results and Discussion

Retrospective tissue oximetry data from 21 sites affected by ulceration were examined in this study to develop the ulcer prediction index. These sites were collectively labeled as "affected" with ulceration. Oximetry data gathered at the affected site were collected, on average, 58 days before the ulcer was first observed at the site. Sensitivity and specificity of the predictive index was tested on data from subjects that developed ulcers (i.e., the foot with the affected site and the contralateral foot) and data from the feet of 21 randomly selected diabetic patients who did not exhibit ulceration during the study period and were collectively labeled as "comparative." Note that in the context of this study, the terms affected or comparative refer to a particular site that did or did not ulcerated and not to a patient that did or did not develop a foot ulcer.

4.1 *Changes at Affected Sites*

Figure 4(a) compares the value of |MD(OXY)| calculated from hyperspectral images of preulcers at 21 affected sites to the average and standard deviation of |MD(OXY)| value calculated over the entire affected foot. To classify pixels in a hyperspectral image as preulcerative or unaffected, the target depicted in Fig. 3(b) was centered on the pixel in question and |MD(OXY)|

and |MD(DEOXY)| were calculated according to Eqs. (4) and (5). In 20 out of 21 preulcer sites, |MD(OXY)| increased at the affected sites when compared to its value averaged over the entire surface of the affected foot. Considerations of the standard deviation establish that |MD(OXY)| and |MD(DEOXY)| are statistically significantly larger in the preulcer regions than over the entire foot. Furthermore, at 13 out of 21 affected sites, the value of |MD(OXY)| was more than one standard deviation larger than its surface average value over the entire foot.

Similarly, Fig. 4(b) compares the values of |MD(DEOXY)| calculated from hyperspectral images of preulcers at 21 affected sites to the mean and standard deviation of |MD(DEOXY)| values calculated over the entire affected foot. Values of |MD(DEOXY)| exhibited a similar but less dramatic pattern as that shown in Fig. 4(a) for |MD(OXY)|. Here, 13 out of 21 affected sites exhibited larger values of |MD(DEOXY)| than its average value calculated over the entire affected foot. Also, 5 out of 21 affected sites exhibited |MD(DEOXY)| values one standard deviation larger than the mean. Figures 4(a) and 4(b) establish that |MD(OXY)| and |MD(DEOXY)| are typically larger in the sites where an ulcer eventually formed. Interpatient variability observed in Fig. 4 can be attributed to differences in diabetic duration, control, and treatment from one subject to another. However, |MD(OXY)| and |MD(DEOXY)| provide a comparison between a target and adjacent regions for the same subject. Furthermore, for diseased tissues they show a remarkable pattern reasonably captured by the threshold |MD(OXY)| and |MD(DEOXY)|.

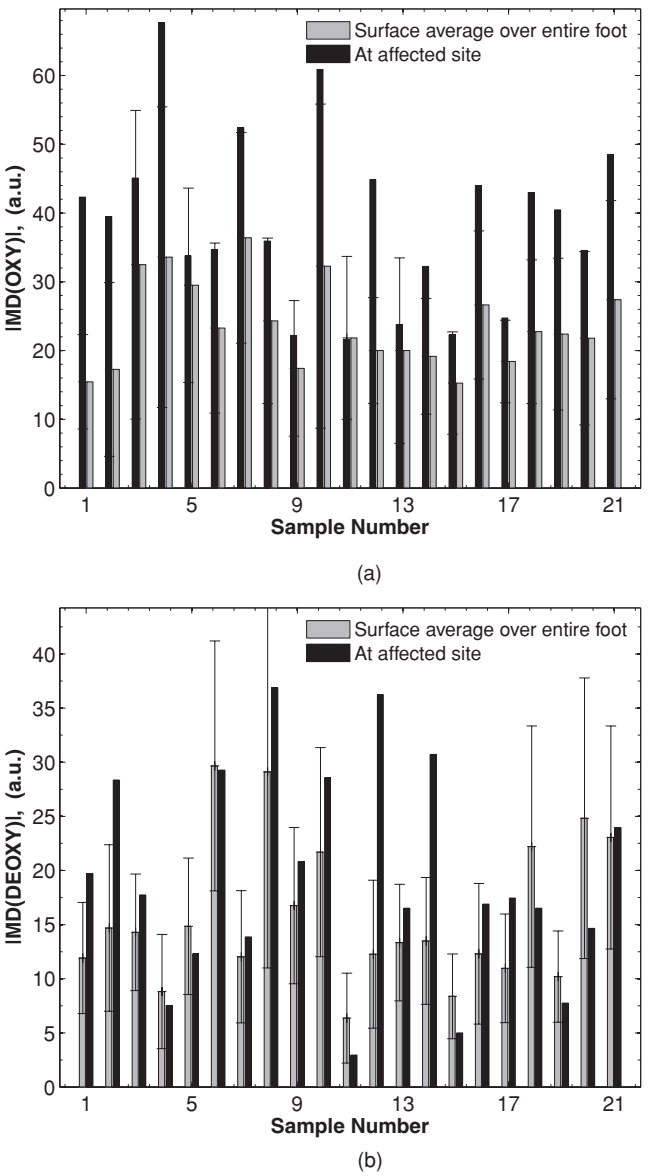

Fig. 4 (a) Values of |MD(OXY)| calculated at the 21 affected sites as well as the mean and standard deviation of |MD(OXY)| values averaged over the entire foot where the ulcer formed. (b) The same plot for |MD(DEOXY)| values. Error bars indicated one standard deviation.

4.2 *Comparison between Affected and Comparative Sites*

Figure 5 plots MD(DEOXY) versus MD(OXY) calculated from preulcer hyperspectral data for 21 affected sites as well as those calculated for the same anatomical location on the contralateral foot and collected during the same visit. Data from 100 random comparative sites on the feet of diabetic patients that never developed ulcers are also shown. Values of MD(OXY) and MD(DEOXY) at the affected sites on the feet of patients who developed ulcers were systematically larger than on those who did not develop ulcers. It is also interesting to note that the MD(OXY) and MD(DEOXY) were larger at affected sites than at the same anatomical location on the contralateral foot. This implies that these changes are specific to preulcerative locations. In addition, they had the same sign corresponding to hyperperfused (both positive) or hypovascular (both negative) tissue. On the other hand, data gathered at the contralateral sites and the comparative group showed no consistency in sign between MD(OXY) and MD(DEOXY) values. In fact, only 3 out

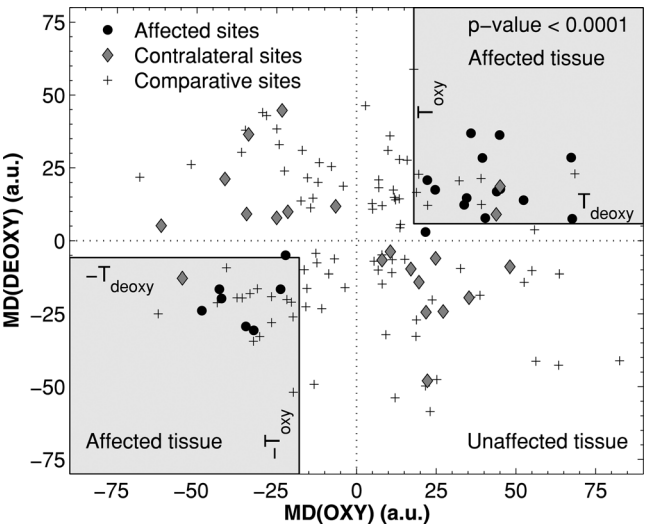

Fig. 5 Scatter plot showing values of MD(OXY) and MD(DEOXY) determined for 21 affected and 21 contralateral sites from diabetic subjects who developed foot ulcers and from 100 random sites fromx diabetic subjects in the comparative groups. Values from affected areas were found to fall inside the gray regions where |MD(OXY)| > 18 and |MD(DEOXY)| > 5.8 with a p-value of <0.0001. Data from contralateral sites were presented for reference and not to serve as a control.

of 21 contralateral sites and roughly half (47 out of 100) of the comparative sites exhibited the same sign between MD(OXY) and MD(DEOXY) values.

Figure 5 also shows gray regions where |MD(OXY)| and |MD(DEOXY)| were greater than the detection thresholds T_{OXY} and T_{DEOXY}, respectively. To determine T_{OXY} and T_{DEOXY}, a skew normal distribution was fit to the |MD(OXY)| and |MD(DEOXY)| values calculated for affected sites and reported in Figs. 4(a) and 4(b), respectively. Then, a single parameter along the skew normal distribution could be used to select a pair of T_{OXY} and T_{DEOXY} values. Data gathered from affected sites fell within the gray region with a p-value of <0.0001 for $T_{OXY} = 18$ and $T_{DEOXY} = 5.8$.

For illustrative purposes, Fig. 6 shows a composite image corresponding to Fig. 3(b), where the polygon overlays indicate that the maximum differences in oxyhemoglobin and deoxyhemoglobin are such that |MD(OXY)| > 18 and |MD(DEOXY)| > 5.8. The approximate location of subsequent ulceration depicted in Fig. 3 is circled. (Color online only.) Figure 6 was generated by transposing the target shown in Fig. 3(b) over each pixel and determining |MD(OXY)| and |MD(DEOXY)|. Note that this procedure does not require prior knowledge of where and if an ulcer will form. Although there are other red overlays, one clearly coincides with the shape and size of the ulcer that eventually formed, as shown in Fig. 3(a). Similar results were obtained at the other affected sites.

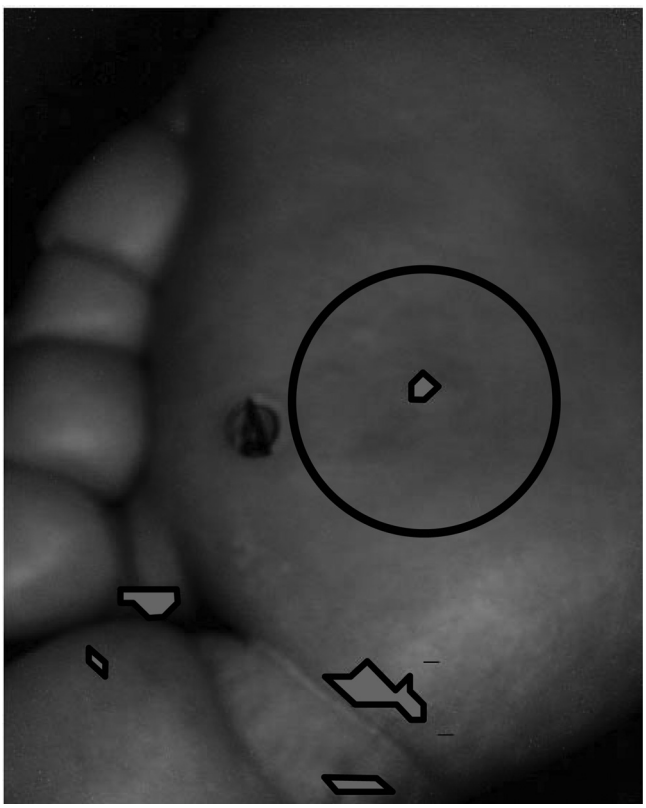

Fig. 6 Composite image corresponding to Fig. 3(b), where the polygon overlays indicate that the maximum differences in oxyhemoglobin and deoxyhemoglobin are such that |MD(OXY)| > 18 and |MD(DEOXY)| > 5.8. The approximate location of subsequent ulceration depicted in Fig. 3 is circled. (Color online only.)

4.3 *Receiver Operating Characteristic Analysis*

Receiver operating characteristic (ROC) analysis was also performed to show the relationship between sensitivity and specificity of the ulcer prediction index for a set of detection thresholds T_{OXY} and T_{DEOXY}. Sensitivity was calculated by dividing the area of skin accurately classified as affected by the total surface area of the affected foot. Specificity was calculated by dividing the total area of skin that was accurately classified as unaffected for comparative subjects by the total area of skin for both feet of affected and comparative subjects. This was done to simulate the application of the ulcer prediction index to a population of diabetic patients at risk of foot ulceration including patients who will not form ulcers. Table 1 summarizes the sensitivity and specificity associated with several values of T_{OXY} and T_{DEOXY}.

Figure 7 shows the ROC curves plotting the sensitivity of the ulcer prediction algorithm versus its specificity for the affected population alone, and the entire population of 21 affected and 21 comparative subjects. The Q-value corresponds to the circled point on the ROC curve (Fig. 7) when sensitivity equals specificity. For an ideal predictor, the Q-value is 100%, whereas it is 50% for a random predictor. The Q-values for the data taken from (*i*) the affected group alone and (*ii*) the comparative and affected groups combined were 85 and 89%, respectively. The combined data from affected and comparative subjects represented a typical population of diabetic patients at risk of developing diabetic foot ulcers that would seek treatment in a diabetic foot clinic. Thus, these data were used to determine the sensitivity and specificity of the present ulcer risk prediction index while the other ROC curve in Fig. 7 is presented for reference. For a high sensitivity of 95%, the specificity was calculated to be 80% for the combined group corresponding to $T_{OXY} = 18$ and $T_{DEOXY} = 5.8$.

The relatively low specificity implies that up to 20% of the foot's surface could be erroneously predicted as preulcerous. Typically, these false-positive predictions occurred over areas already known to be at risk for ulceration, such as toes or plantar surface. Such false positives may evoke unnecessary concern for the patient or care giver. Thus, effort should be made to further increase the specificity. This may be achieve by detecting structural changes in the skin[34,35] that preempt ulceration, such as collagen scarring, inflammation, or changes in epidermal thickness.[36–38] However, this analysis falls outside the scope of the present study.

Table 1 Summary of the sensitivity and specificity associated with several values of thresholds of several T_{OXY} and T_{DEOXY} .

T_{OXY}	T_{DEOXY}	Sensitivity	Specificity
15.3	3.8	100%	72%
18.0	5.8	95%	80%
29.7	13.1	87%	89%
40.1	21.2	67%	94%
70.9	45.8	0%	100%

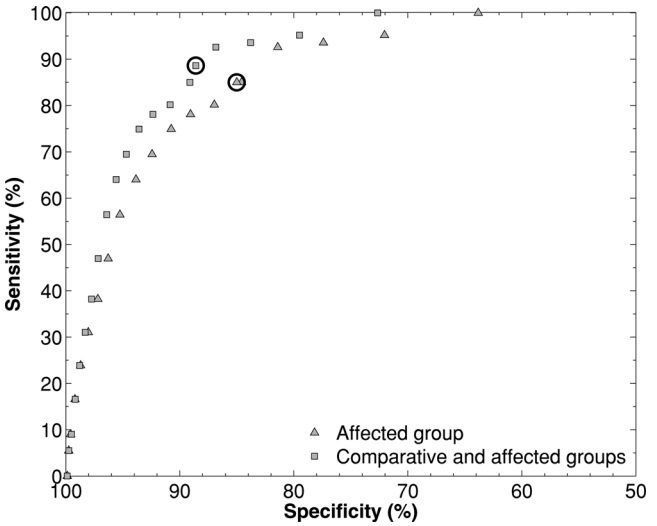

Fig. 7 ROC curve showing the sensitivity versus specificity of the ulcer prediction algorithm. Sensitivity was assessed for data from diabetic subjects who developed foot ulcers and the contralateral foot (affected group). The specificity was calculated for data from the feet of the affected subjects alone and then the comparative and affected subjects combined.

5 Conclusion

This study demonstrated the ability of hyperspectral imaging between 500 and 650 nm to assess the risk of diabetic foot ulcer development. It also established that hyperspectral tissue oximetry has the ability to identify ischemic and inflammatory complications before they are visible during a clinical examination. Retrospective analysis of hyperspectral tissue oximetry from preulcerative locations showed that diabetic foot ulcer formation can be predicted with a sensitivity and specificity of 95 and 80%, respectively. Thus, hyperspectral imaging could provide the diabetes care giver with information necessary to treat and possibly prevent foot complications earlier and noninvasively. A prospective study combining the present algorithm with preventative care[39] would prove the effectiveness of the present algorithm in reducing diabetic foot ulcer formation.

Acknowledgments

This research was funded in part through a grant from the National Institute of Diabetes and Digestive and Kidney Diseases (Grant No. R42-DK069871). We thank Wendy Arriaga and Gustavo Chavez from Olive View who have been extremely helpful with data collection.

References

1. S. Wild, G. Roglic, A. Green, R. Sicree, and H. King, "Global prevalence of diabetes," *Diabetes Care* **27**(5), 1047–1053 (2004).
2. J. E. Shaw, R. A. Sicree, and P. Z. Zimmet, "Global estimates of the prevalence of diabetes for 2010 and 2030," *Diabetes Res. Clin. Practice* **87**(1), 4–14 (2010).
3. G. E. Reiber, "The epidemiology of diabetic foot problems," *Diabetic Med.* **13**(S1), 6–11 (1996).
4. A. J. M. Boulton, D. G. Armstrong, S. F. Albert, R. G. Frykberg, R. Hellman, M. S. Kirkman, L. A. Lavery, J. W. LeMaster, J. L. Mills Sr., M. J. Mueller, P. Sheehan, and D. K. Wukich, "Comprehensive foot examination and risk assessment," *Diabetes Care* **31**(5), 1679–1685 (2008).
5. R. E. Pecoraro, G. E. Reiber, and E. M. Burgess, "Pathways to diabetic limb amputation. Basis for prevention," *Diabetes Care* **13**(5), 513–521 (1990).
6. R. G. Frykberg, T. Zgonis, D. G. Armstrong, V. R. Driver, J. M. Giurini, S. R. Kravitz, A. S. Landsman, L. A. Lavery, J. C. Moore, J. M. Schuberth, D. K. Wukich, C. Andersen, and J. V. Vanore, "Diabetic foot disorders: a clinical practice guideline (2006 revision)," *J. Foot Ankle Surg.* **45**(5S), 1–66 (2006).
7. C. Harrington, M. J. Zagari, J. Corea, and J. Klitenic, "A cost analysis of diabetic lower-extremity ulcers," *Diabetes Care* **23**(9), 1333–1338 (2000).
8. S. D. Ramsey, K. Newton, D. Blough, D. K. McCulloch, N. Sandhu, G. E. Reiber, and E. H. Wagner, "Incidence, outcomes, and cost of foot ulcers in patients with diabetes," *Diabetes Care* **22**(3), 382–387 (1999).
9. L. A. Lavery, D. G. Armstrong, S. A. Vela, T. L. Quebedeaux, and J. G. Fleischli, "Practical criteria for screening patients at high risk for diabetic foot ulceration," *Arch. Intern. Med.* **158**(2), 157–162 (1998).
10. H. M. Rathur and A. J. M. Boulton, "The diabetic foot," *Clin. Dermatol.* **25**(1), 109–120 (2007).
11. L. Belbridge, G. Ctercteko, C. Fowler, T. S. Reeve, and L. P. Le Quesne, "The aetiology of diabetic neuropathic ulceration of the foot," *Br. J. Surg.* **72**(1), 1–6 (1985).
12. P. J. Palumbo and L. J. Melton, "Peripheral vascular disease and diabetes," in *Diabetes in America*, 2nd Ed., *Chap. 17*, U.S. Government Printing Office, Washington, DC (1985), pp. 1–21 (NIH publication no. 85-1468).
13. K. J. Zuzak, M. D. Schaeberle, E. N. Lewis, and I. W. Levin, "Visible reflectance hyperspectral imaging: characterization of a noninvasive, *in-vivo* system for determining tissue perfusion," *Anal. Chem.* **74**(9), 2021–2028 (2002).
14. L. Kocsis, P. Herman, and A. Eke, "The modified Beer-Lambert law revisited," *Phys. Med. Biol.* **51**(5), 91–98 (2006).
15. V. V. Tuchin, S. R. Utz, and I. V. Yaroslavsky, "Tissue optics, light distribution, and spectroscopy," *Opt. Eng.* **33**, 3178–3188 (1994).
16. J. C. Finlay and T. H. Foster, "Hemoglobin oxygen saturations in phantoms and in vivo from measurements of steady-state diffuse reflectance at a single, short source-detector separation," *Med. Phys.* **31**(7), 1949–1959 (2004).
17. P. J. Dwyer and C. A. DiMarzio, "Hyperspectral imaging for dermal hemoglobin spectroscopy," *Proc. SPIE* **3752**, 72–82 (July 1999).
18. A. Nouvong, B. Hoogwerf, E. Mohler, B. Davis, A. Tajaddini, and E. Medenilla, "Evaluation of diabetic foot ulcer healing with hyperspectral imaging of oxyhemoglobin and deoxyhemoglobin," *Diabetes Care* **32**(11), 2056–2061 (2009).
19. L. Khaodhiar, T. Dinh, K. T. Schomacker, S. V. Panasyuk, J. E. Freeman, R. Lew, T. Vo, A. A. Panasyuk, C. Lima, J. M. Giurini, T. E. Lyons, and A. Veves, "The use of medical hyperspectral technology to evaluate microcirculatory changes in diabetic foot ulcers and to predict clinical outcomes," *Diabetes Care* **30**(4), 903–910 (2007).
20. R. Gillies, J. E. Freeman, L. C. Cancio, D. Brand, M. Hopmeier, and J. R. Mansfield, "Systemic effects of shock and resuscitation monitored by visible hyperspectral imaging," *Diabetes Technol. Therapeut.* **5**(5), 847–855 (2003).
21. A. Sassaroli and S. Fantini, "Comment on the modified Beer-Lambert law for scattering media," *Phys. Med. Biol.* **49**, 255–257 (2004).
22. V. V. Tuchin, *Tissue Optics: Light Scattering Methods and Instruments for Medical Diagnosis*, SPIE Bellingham, WA (2007).
23. M. J. C. Van Gemert, S. L. Jacques, H. Sterenborg, and W. M. Star, "Skin optics," *IEEE Trans. Biomed. Eng.* **36**(12), 1146–1154 (1989).
24. R. R. Anderson and J. A. Parrish, "The optics of human skin," *J. Invest. Dermatol.* **77**(1), 13–19 (1981).
25. V. Twersky, "Absorption and multiple scattering by biological suspensions," *J. Opt. Soc. Am.* **60**(8), 1084–1093 (1970).
26. V. V. Tuchin, *Tissue Optics: Light Scattering Methods and Instruments for Medical Diagnosis*, SPIE Press, Bellingham, WA (2007).
27. S. Wray, M. Cope, D. T. Delpy, J. S. Wyatt, and E. O. Reynolds, "Characterization of the near infrared absorption spectra of cytochrome

aa3 and haemoglobin for the non-invasive monitoring of cerebral oxygenation," *Biochim. Biophys. Acta Bioenerget.* **933**(1), 184–192 (1988).
28. A. P. Harris, M. J. Sendak, R. T. Donham, M. Thomas, and D. Duncan, "Absorption characteristics of human fetal hemoglobin at wavelengths used in pulse oximetry," *J. Clin. Monitor. Comput.* **4**(3), 175–177 (1987).
29. S Takatani and D. Graham, M., "Theoretical analysis of diffuse reflectance from a two-layer tissue model," *IEEE Trans. Biomed. Eng.* **26**(12), 656–664 (1979).
30. D. W. Marquardt, "An algorithm for least-squares estimation of nonlinear parameters," *J. Soc. Ind. Appl. Math.* **11**(2), 431–441 (1963).
31. G. Zonios, J. Bykowski, and N. Kollias, "Skin melanin, hemoglobin, and light scattering properties can be quantitatively assessed *in vivo* using diffuse reflectance spectroscopy," *J. Invest. Dermatol.* **117**(6), 1452–1457 (2001).
32. A. A. Gowen, C. P. O'Donnell, P. J. Cullen, G. Downey, and J. M. Frias, "Hyperspectral imaging–an emerging process analytical tool for food quality and safety control," *Trends Food Sci. Technol.* **18**(12), 590–598 (2007).
33. G. N. Stamatas, C. J. Balas, and N. Kollias, "Hyperspectral image acquisition and analysis of skin," *Proc. SPIE* **4959**, 77–82 (2003).
34. D. Yudovsky and L. Pilon, "Rapid and accurate estimation of blood Saturation, melanin content, and epidermis thickness from spectral diffuse reflectance," *App. Opt.* **49**(10), 1707–1719 (2010).
35. D. Yudovsky and L. Pilon, "Approximate expression for diffuse reflectance of semi-infinite and two-layer absorbing and scattering media," *Appl. Opt.* **48**(35), 6670–6683 (2009).
36. M. W. Ferguson, S. E. Herrick, M. J. Spencer, J. E. Shaw, A. J. Boulton, and P. Sloan, "The histology of diabetic foot ulcers," *Diabetic Med.* **13**, 30–33 (1996).
37. J. S. Vande Berg and R. Rudolph, "Pressure (decubitus) ulcer: variation in histopathology—a light and electron microscope study," *Human Pathol.* **26**(2), 195–200 (1995).
38. J. A. Witkowski and L. C. Parish, "Histopathology of the decubitus ulcer," *J. Am. Acad. Dermatol.* **6**(6), 1014–1021 (1982).
39. J. Apelqvist, K. Bakker, W. H. van Houtum, M. H. Nabuurs-Franssen, and N. C. Schaper, "International consensus and practical guidelines on the management and the prevention of the diabetic foot," *Diabetes/Metab. Res. Rev.* **16**(1), 84–92 (2000).